Advanced Composite Materials
Publication details, including instructions for authors and subscription information:
http://www.tandfonline.com/loi/tacm20

Impurity Tracing in Nanostructured Al and Al/Al2O3 Composite Prepared by High Energy Milling

S. S.Razavi Tousi [a] , R.Yazdani Rad [b] & M. S. Abdi [c]

[a] Materials and Energy Research Center, P.O. Box 31787/316, Karaj, Iran

[b] Materials and Energy Research Center, P.O. Box 31787/316, Karaj, Iran

[c] Ceramic Engineering Department, Malayer University, Malayer, Iran

Version of record first published: 02 Apr 2012.

To cite this article: S. S.Razavi Tousi , R.Yazdani Rad & M. S. Abdi (2010): Impurity Tracing in Nanostructured Al and Al/Al2O3 Composite Prepared by High Energy Milling, Advanced Composite Materials, 19:4, 393-402

To link to this article: http://dx.doi.org/10.1163/092430410X504206

VSP

Advanced Composite Materials 19 (2010) 393–402

ADVANCED COMPOSITE MATERIALS
brill.nl/acm

Impurity Tracing in Nanostructured Al and Al/Al_2O_3 Composite Prepared by High Energy Milling

S. S. Razavi Tousi [a], **R. Yazdani Rad** [a,*] **and M. S. Abdi** [b]

[a] Materials and Energy Research Center, P. O. Box 31787/316, Karaj, Iran
[b] Ceramic Engineering Department, Malayer University, Malayer, Iran

Received 25 February 2009; accepted 29 November 2009

Abstract
The nature and origins of major impurities and their effect on properties of a nano-grained Al and Al/Al_2O_3 composite prepared in a planetary ball mill have been investigated. Carbon and oxygen from the process control agent and Fe from the vial erosion were found to be the main impurities affecting the structural properties, such as lattice parameters and melting point of the milled aluminum mixture. An attempt was made to assess the effect of impurities on mechanical properties of the products using common theoretical formulas.

Keywords
Nanostructured materials, mechanical alloying, metal matrix composites

1. Introduction

Mechanical alloying (MA) as a well known method for production of advanced materials usually suffers from the problem of contaminations [1–3]. Three major sources of contamination are: atmosphere, container and process control agent (PCA). The contaminations caused by atmosphere are usually avoided using an inert gas or vacuum, but addition of PCA in the metallic systems and erosion of balls/container are inevitable. Effects of impurities on the structural properties of the milled materials have been investigated in several works [4–19].

The presence of contaminations is deemed to be a detrimental phenomenon in various applications, such as its negative effects on the electrical properties of the thermoelectric materials produced by mechanical alloying [9, 10], negative effect on the H-storage [11] and delaying the synthesis of the nano-crystalline materials [12].

* To whom correspondence should be addressed. E-mail: ryazdani5@gmail.com.

 DOI:10.1163/092430410X504206

However, it could be welcomed in some minor usages such as increasing the thermal stability of nano-crystalline materials [13], accelerating the synthesis of the nano-crystalline materials [14], improving the sintering properties [16], increasing the electrocatalytic performance of alloy electrodes [15] and improving the mechanical properties of the milled products [17–19].

Such diverse concepts of the influences caused by the contaminations highlight the importance of tracing the impurities in the mechanical alloying systems. The amounts, position and structural effects of contaminations caused by the vial and PCA in monolithic Al and Al matrix composite during milling stages will be studied in this work. Similar to Benjamin and Bamford's findings [18], results show that a distribution of the fine oxide and carbide particles introduced by the decomposition of PCA has a positive effect on the mechanical properties of the Al matrix.

2. Experimental Procedure

Commercial purity Al powder (Merck, Art. No: 1056) as a monolithic system and a mixture of Al-20 wt% alumina powder (Martinswerk, MR70, d50: 0.5–0.8 μm) were separately milled in a P5 planetary mill for various periods of time up to 25 h. The ball to powder ratio was 15:1 and the mill speed was maintained at 250 RPM. Three wt% of stearic acid was added as PCA. The milling atmosphere was Ar and the product sampling was performed in a glove box to prevent oxidation. A Philips CM 200 FEG transmission electron microscopy (TEM) was used to detect the formation of nanometric carbide and oxide particles introduced by the PCA decomposition. The melting point of the powders was obtained using differential thermal analysis (DTA) with a heating rate of 10°C/min. The powders were pressed by a uniaxial cold press (1 GPa) and then sintered at 640°C for 30 min in the Ar atmosphere using a tube furnace. Consequently tablet bulk samples of 95%–100% theoretical density were obtained. A fracture test was carried out on the bulk samples with a strain rate of 3.3×10^{-2} (s^{-1}). The samples were examined using a Cambridge (Stereo Scan S360) scanning electron microscope (SEM) operating at a voltage of 30 kV and a Philips (PW3710) diffractometer (30 kV and 25 mA) with Cu K_α radiation. Grain size of samples was calculated by the Williamson–Hall formula [20].

In order to minimize the errors caused by aberration of 2θ variation, the Nelson–Riely method was used to calculate lattice parameter of Al for at least three peaks using equation (1) [21]

$$F(\theta) = 0.5(\cos^2\theta/\sin^2\theta + \cos^2\theta/\theta). \tag{1}$$

The minor errors caused by peak position displacement and peak shape deformation were diminished by the following procedure: the position of each peak assigned to the middle of three $P_{x/y}$ with x/y equal to 0.6, 0.8 and 1, the final peak position was obtained by averaging these values. Full details of this method are described in Ref. [22].

3. Result and Discussion

3.1. Structural Properties

Employing the Nelson–Riely approach, the lattice parameter of Al was measured in the monolithic system (Fig. 1). The lattice parameter of the as-received Al (0.40465 nm) is lower than the value of the pure Al (0.4049 nm). This can be explained by the presence of a minor amount of impurities such as Fe and Zn (Table 1). Since the atomic radii of Fe (0.126 nm) and Zn (0.138 nm) are lower than that of Al (0.143 nm), the presence of these elements in solid solution reduces the lattice parameter of Al.

Several factors are known to affect the lattice parameter during milling [23–26]. The increase can be ascribed to the thermo-mechanical decomposition of PCA and to the elemental carbon and oxygen followed by an interstitial placement of these elements in the Al lattice. Further milling results in a gradual reduction that can be ascribed to three factors:

(a) Decrease in grain size is known as a reason for the diminution of lattice parameter with milling time. This can be explained by the compressive stress exerted by the grain surface onto the bulk of the grains [24, 25].

(b) The abrasion of the balls and vial introduces impurity. Fe content in the monolithic Al powder increases by 0.4% after completion of the milling process (Table 1). Due to the intense impacts followed by the formation of rapid diffu-

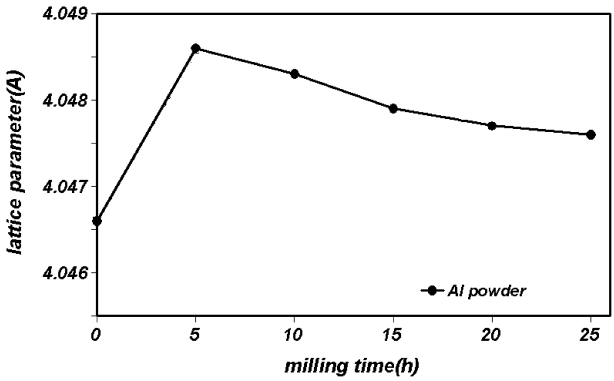

Figure 1. Effect of milling time on the lattice parameter of monolithic Al.

Table 1.
Quantitative elemental analysis of the as-received and milled Al powders

	Zn	Ni	Cr	Fe	Ti	Cu	Mn
As-received Al (%)	0.021	0.003	<0.004	0.42	0.008	0.0007	<0.01
Milled monolithic Al (%)	0.017	0.092	<0.004	0.87	0.01	0.046	0.128

sion tracks, debris of stainless steel was dissolved in the Al lattice. The smaller atomic radius of Fe and Mn (0.126 nm) compared to Al reduced the lattice parameter.

(c) Escape of the decomposed PCA atoms in the form of gas or formation of aluminum carbide and oxide particles in the matrix. TEM observation confirms presence of these carbide and oxide particles in the reinforced Al particles milled up to 25 h (Fig. 2).

The small grain size (46 nm) [27], high density of dislocations and imperfections, as well as presence of O, C and Fe in solid solution decrease the stability of the Al lattice. Table 2 shows the effect of milling time on the Fe impurity of the composite powders. Accordingly, diminution of melting point of Al in the case of composite powder was detected by DTA (Fig. 3).

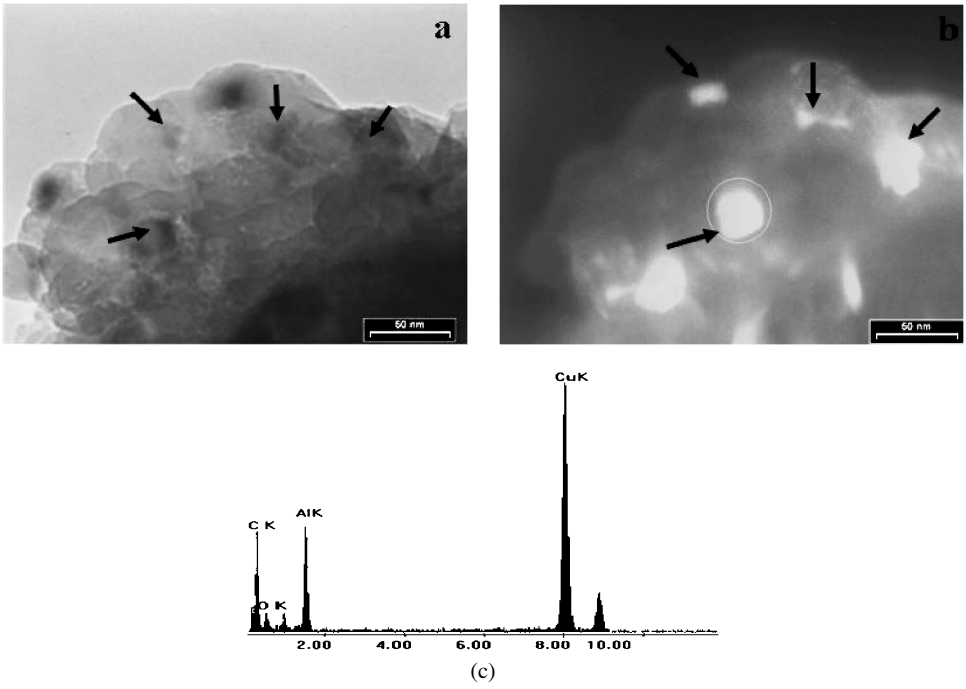

Figure 2. Presence of nanometeric particles within Al matrix; (a) bright field, (b) dark field and (c) EDS image of one of these particles.

Table 2.
Effect of milling time on the Fe impurity of the composite powders

Milling time (h)	0	5	10	15	20	25
Fe (%)	0.42	1.49 ± 0.53	1.786 ± 0.35	2.018 ± 0.4	2.48 ± 0.17	2.65 ± 0.47

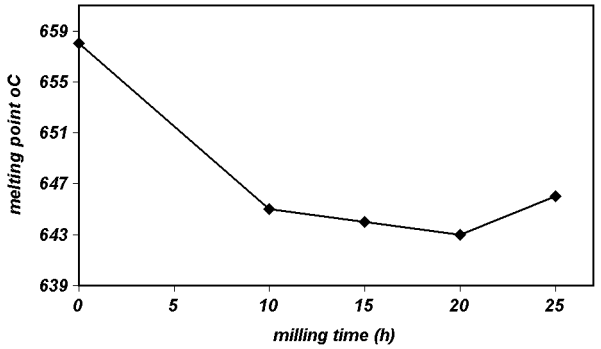

Figure 3. Effect of milling time on the melting point of the reinforced powders.

Sintering at 640°C for 30 min has no considerable effect on the grain growth of Al. This can be explained by the Zenner pinning effect from the nanometric oxide and carbide particles which act as barriers to the motion of the grain boundaries [28].

Another reason is the presence of Fe impurity as solid solution in the Al lattice. Grain boundary energy can be decreased by the accumulation of the Fe atoms [29, 30].

By migration of the boundaries, the concentration of Fe atoms in the boundary regions increases, and hence the driving force for boundary migration, i.e., grain boundary energy reduces. Accordingly, using the Williamson–Hall formula, one can find that the grain size is fixed in a value of 70 nm.

Low magnification SEM images of the bulk sample produced from the Al powder milled for 5 h show that the surface of the weak sintered particles is a preferred place for initiation of cracks (Fig. 4(a) and 4(b)). Indeed, the presence of a thin layer of alumina on the surface of the initial Al particles reduces the cohesive strength of the material at the particle boundaries. This promotes a decohesive rupture mechanism [31].

On the other hand, due to the presence of a high volume fraction of the grain boundary phase, another suitable region for crack propagation must be considered [32–34]. In the nano-crystalline (NC) regime the spatial confinement of the grains below several tens of nanometres inhibits the operation of dislocation sources inside grains, limiting the plastic deformation [35, 36]. It is expected that in NC metals plastic deformation can be accommodated by the grain boundaries [37]. Since grain boundaries contain the lowest melting point of an alloy system and are easy paths for diffusion and sites for segregation, cracks propagate along the grain boundaries and, thus, an intergranular fracture is anticipated in the nano-crystalline materials. Figure 4(c) shows that creation of fracture surface has proceeded along the grain boundaries, resulting in a different mode of intergranular fracture accompanied by the decohesive rupture. The grain size is in agreement with the result of the Williamson–Hall formula.

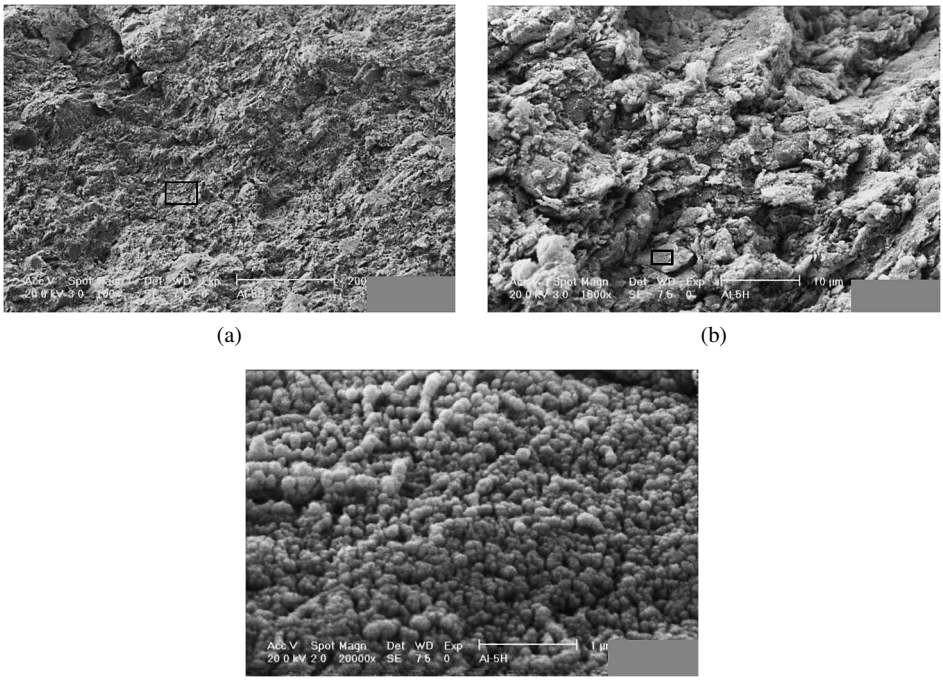

Figure 4. Fracture surface of the bulk sample produced from the monolithic Al powder milled for 5 h.

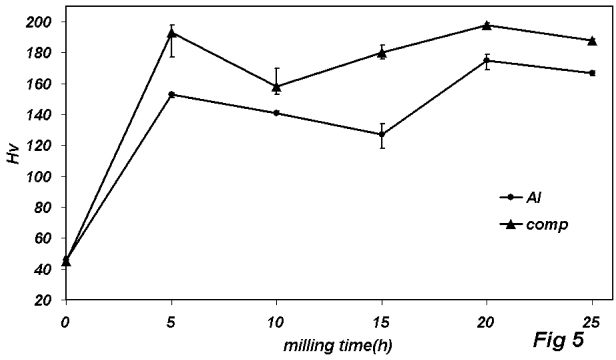

Figure 5. Hardness of the monolithic and composite powders *vs* milling time.

3.2. Mechanical Properties

A fine grained structure has a great influence on the hardness due to the Hall–Petch relation (Fig. 5). For a pure nano-crystalline Al sample, Z. N. Farhat *et al.* proposed equation (2) as the Hall–Petch formula [38], which was based on the obtained hardness values *vs* grain size between 15–100 nm:

$$H\ (\text{MPa}) = 34\ (\text{MPa}) + 0.21\ (\text{MPa m}^{0.5}) d^{-0.5}\ (\text{m}^{-0.5}). \qquad (2)$$

For a pure Al sample with a grain size of 70 nm, the hardness value was calculated to be 80 H_v, which is about half the experimental values obtained in this work. Obviously, grain boundary strengthening is not the only mechanism responsible for the increase in the hardness of the milled Al. The sintering process provides a sufficient driving force for dislocations to reach grain boundaries; thus, strain hardening also cannot take on this excessive value of the hardness.

The presence of the aluminum carbide and oxide particles in the Al matrix provides another strengthening agent. Although the PCA (stearic acid) decomposes completely during milling [39], not all the decomposition products necessarily take part in the reaction with Al. A perfect reaction of 3 wt% stearic acid ($C_{17}H_{35}COOH$) with Al, would produce 10.8% by volume of Al_4C_3 and Al_2O_3 particles. The relation between inter-particle spacing, λ, particle size, d, and volume fraction, V, of the reinforcements is given by equation (3) [40]:

$$\lambda = \left(\frac{6\,\mathrm{V}}{\pi}\right)^{-1/3} \times d. \tag{3}$$

Assuming spherical dispersoids with a average size of 30 nm (Fig. 2), the inter-particle spacing would be obtained as 51 nm; this would improve strength by 875 MPa according to the Orowan equation [41]:

$$\Delta\sigma = m\left(\frac{0.84Gb}{\lambda - d}\right), \tag{4}$$

where m is 3.06 for fcc metals, G, shear modulus and b the Burger's vector of Al. In the absence of appreciable work hardening, the hardness of a material, H_v, as measured using a pyramidal indenter is proportional to the yield stress, $H_v \approx 3\sigma$ [42]. Therefore, the increase in the yield stress is worked out to be $\Delta H_v = 262$. Considering the hardness of 25 h milled Al, 150 H_v and the contribution from the grain boundary strengthening, 80 H_v, the strengthening attributed to the dispersoids would be 223 MPa, which arises from a particle spacing of 112 nm if calculated using equation (4). Considering a particle spacing of 112 nm and using equation (3), only 10% of the decomposed PCA has reacted with Al. Due to the negative ΔG of formation of Al_2O_3 and Al_4C_3, existence of C and O atoms in the interstitial position after annealing is unlikely. Therefore, the residual oxygen and carbon probably left the system as CO_2, CH_4 or H_2O, which is known as degassing in the MA process.

In the case of composite samples, well homogenized distribution of the alumina particles in the Al matrix after 15 h milling was achieved (Fig. 6). Assuming $d \approx 400$ nm according to the SEM images, the inter-particle spacing from equation (3) would be 615 nm which is in agreement with Fig. 6. According to equation (4), strengthening arisen from the alumina particles is 86 MPa, this improves the hardness by 25 H_v. Sum of the hardness values caused by grain boundaries, the nano-dispersoids generated by PCA and submicron alumina is 175 H_v, which is lower than the experimental value (185 H_v). This discrepancy is ascribed to the presence of iron in the form of solid solution or compounds with Al.

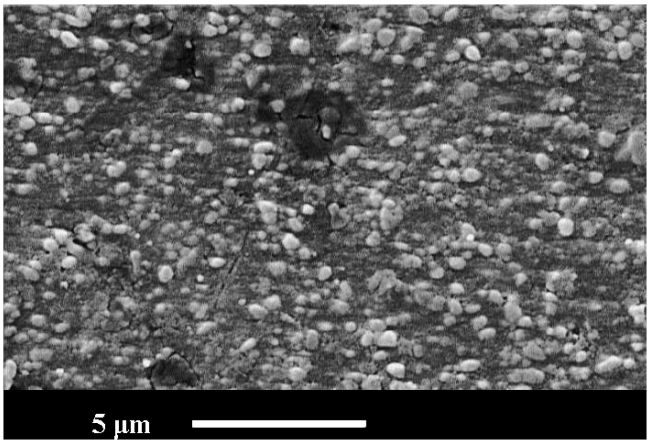

Figure 6. Distribution of reinforcement particles within Al matrix.

4. Conclusion

The effects of impurities on the structural properties of monolithic Al and Al-20 wt% were studied. Lattice parameter and melting point were affected by Fe, C and O impurities as well as reduction in grain size. Part of PCA decomposition products remained in the system and its major part exited during degassing. According to the theoretical expression, the effect of nanostructured matrix and the reinforcement created by PCA is much larger than the one caused by the addition of the submicron α-alumina particles.

References

1. C. Suryanarayana, Mechanical alloying and milling, *Prog. Mater. Sci.* **46**, 1–184 (2001).
2. C. C. Koch, Synthesis of nanostructured materials by mechanical milling: problems and opportunities, *Nanostruct. Mater*. **9**, 13–22 (1997).
3. L. He and E. Ma, Nanophase metallic alloys consolidated from powders prepared by mechanical alloying, *Mater. Sci. Engng A* **204**, 240–245 (1995).
4. M. Zhua, L. Z. Ouyanga, Z. F. Wua, M. Q. Zenga, Y. Y. Lia and J. Zoub, The effect of Cu addition and milling contaminations on the microstructure evolution of ball milled Al–Pb alloy during sintering, *Mater. Sci. Engng A* **434**, 352–359 (2006).
5. Q. Zeng and I. Baker, Magnetic properties and thermal ordering of mechanically alloyed Fe–40 at% Al, *Intermetallics* **14**, 396–405 (2006).
6. C. Goujon, P. Goeuriot, P. Delcroix and G. L. Caër, Mechanical alloying during cryomilling of a 5000 Al alloy/AlN powder: the effect of contamination, *J. Alloys Compounds* **315**, 276–283 (2001).
7. J. Alkebro, S. Begin-Colin, A. Mocellin and R. Warren, Mechanical alloying of alumina ± yttria powder mixtures, *J. Eur. Ceramic Soc*. **20**, 2169–2174 (2000).
8. B. B. Fernandes, G. Rodrigues, G. C. Coelho and A. S. Ramos, On iron contamination in mechanically alloyed Cr–Si powders, *Mater. Sci. Engng A* **405**, 135–139 (2005).

9. J. De, A. M. Umarji and K. Chattopadhyay, Origin of contamination and role of mechanochemistry during mechanical alloying: the case of Ag–Te alloys, *Mater. Sci. Engng A* **449–451**, 1062–1066 (2007).
10. T. Dasgupta and A. M. Umarji, Role of milling parameters and impurity on the thermoelectric properties of mechanically alloyed chromium silicide, *J. Alloys Compounds* (2007).
11. J. R. Ares, K.-F. Aguey-Zinsou, T. Klassen and R. Bormann, Influence of impurities on the milling process of MgH2, *J. Alloys Compounds* **434–435**, 729–733 (2007).
12. P. Bhattacharya, P. Bellon, R. S. Averback and S. J. Hales, Nanocrystalline TiAl powders synthesized by high-energy ball milling: effects of milling parameters on yield and contamination, *J. Alloys Compounds* **368**, 187–196 (2004).
13. R. Juárez, J. J. Sũnol, R. Berlanga, J. Bonastre and L. Escoda, The effects of process control agents on mechanical alloying behavior of a Fe–Zr based alloy, *J. Alloys Compounds* **434–435**, 472–476 (2007).
14. J. Joardar, S. K. Pabi and B. S. Murty, Milling criteria for the synthesis of nanocrystalline NiAl by mechanical alloying, *J. Alloys Compounds* **429**, 204–210 (2007).
15. M. A. Domínguez-Crespo, M. Plata-Torres, A. M. Torres-Huerta, I. A. Ortiz-Rodríguez, C. Ramírez-Rodríguez and E. M. Arce-Estrada, Influence of Fe contamination and temperature on mechanically alloyed Co–Ni–Mo electrodes for hydrogen evolution reaction in alkaline water, *Mater. Character*. **56** 138–146 (2006).
16. C. B. Reid, J. S. Forrester, H. J. Goodshaw, E. H. Kisi and G. J. Suaning, A study in the mechanical milling of alumina powder, *Ceramics Intl* **34** 1551–1556 (2008).
17. H. Kurishita, T. Kuwabara and M. Hasegawa, Development of ultra-fine grained V–W–Y alloys with superior mechanical properties by effective usage of WC debris introduced during mechanical alloying, *Mater. Sci. Engng A* **432**, 245–252 (2006).
18. J. S. Benjamin and M. J. Bamford, Dispersion strengthened aluminum made by mechanical alloying, *Metallurgical Trans. A* **8**, 1301–1305 (1997).
19. S. Ohtsuka, S. Ukai, M. Fujiwara, T. Kaito and T. Narita, Nano-structure control in ODS martensitic steels by means of selecting titanium and oxygen contents, *J. Phys. Chem. Solids* **66**, 571–575 (2005).
20. G. K. Williamson and W. H. Hall, X-ray line broadening from filed Al and W, *Acta Metall.* **1**, 22–31 (1953).
21. J. B. Nelson and D. P. Riley, An experimental investigation of extrapolation methods in the derivation of accurate unit–cell dimensions of crystals, *Proc. Phys. Soc. (London)* **57**, 160–176 (1945).
22. P. K. Harold and L. E. Alexander, *X-Ray Diffraction Procedure*. Wiley, New York, USA (1954).
23. Y. Duan and J. Li, Structure study of nickel nanoparticles, *Mater. Chem. Phys*. **87**, 452–454 (2004).
24. A. Korchef, Y. Champion and N. Njah, X-ray diffraction analysis of aluminum containing Al_8Fe_2Si processed by ECAP, *J. Alloys Compounds* **427**, 176–182 (2007).
25. M. Liu, B. Shi, J. Guo, X. Cai and H. Song, Lattice constant dependence of elastic modulus for ultrafine grained mild steel, *Scripta Materialia* **49**, 167–171 (2003).
26. A. M. Tonejc and I. Djerdj, An analysis of evolution of grain size-lattice parameter dependence in nanocrystalline TiO_2 anatase, *Mater. Sci. Engng C* **19**, 85–89 (2002).
27. S. S. Razavi Tousi, R. Yazdani Rad, E. Salahi, I. Mobasherpour and M. Razavi, Production of Al–20 wt.% Al_2O_3 composite powder using high energy milling, *Powder Technol.* **192** 346–351 (2009).
28. C. S. Smith, in: C. Zener, Grains, phases and interfaces: an interpretation of microstructure, *Trans. Metall. Soc. AIME* **175**, 15–51 (1948).

29. R. Kirchheim, Grain coarsening inhibited by solute segregation, *Acta Materialia* **50**, 413–419 (2002).
30. F. Liu and R. Kirchheim, Grain boundary saturation and grain growth, *Acta Materialia* **51**, 521–525 (2004).
31. K. Mills, *Fractography*. ASM Handbook, USA (1992).
32. L. Hongqi and F. Ebrahimi, Ductile to brittle transition in nanocrystalline metals, *Adv. Mater*. **17**, 1969–1972 (2005).
33. H. Li and F. Ebrahimi, Tensile behavior of a nanocrystalline Ni–Fe alloy, *Acta Materialia* **54** 2877–2886 (2006).
34. A. Hasnaoui, H. Van Swygenhoven and P. Derlet, Dimples on nanocrystalline fracture surfaces as evidence for shear plane formation, *Science* **300**, 1550–1555 (2003).
35. K. S. Kumar, H. V. Swygenhoven and S. Suresh, Mechanical behavior of nanocrystalline metals and alloys, *Acta Materialia* **53**, 5743–5774 (2003).
36. H. Iwasaki, K. Higashi and T. G. Nieh, Tensile deformation and microstructure of a nanocrystalline Ni–W alloy produced by electrodeposition, *Scripta Materialia* **50**, 395–399 (2004).
37. M. A. Meyers, A. Mishra and D. J. Benson, Mechanical properties of nanocrystalline materials, *Prog. Mater. Sci.* **51**, 427–556 (2006).
38. Z. N. Farhat, Y. Ding, D. O. Northwood and A. T. Alpas, Effect of grain size on friction and wear of nanocrystalline aluminum, *Mater. Sci. Engng A* **206**, 302–313 (1995).
39. S. Kleiner, F. Bertocco, F. A. Khalid and O. Beffort, Decomposition of process control agent during mechanical milling and its influence on displacement reaction in the Al–TiO_2 system, *Mater. Chem. Phys*. **89**, 362–366 (2005).
40. Z. Y. Ma, Y. L. Li, Y. Liang, F. Zheng, J. Bi and S. C. Tjong, Nanometric Si_3N_4 particulate-reinforced aluminum composite, *Mater. Sci. Engng A* **219**, 229–231 (1996).
41. U. F. Kocks, A statistical theory of flow stress and work hardening, *Phil. Mag*. **13**, 541–566 (1966).
42. M. F. Ashby and D. R. H. Jones, *Engineering Materials 1*. Pergamon Press (1980).